**Article:**
Lu, J, Kumar Mishra, P, Hunter, TN et al. (2022) Functionalization of mesoporous carbons derived from pomelo peel as capacitive electrodes for preferential removal/recovery of copper and lead from contaminated water. Chemical Engineering Journal, 433 (1). 134508. ISSN: 1385-8947

https://doi.org/10.1016/j.cej.2022.134508

# Functionalization of mesoporous carbons derived from pomelo peel as capacitive electrodes for preferential removal/recovery of copper and lead from contaminated water

Jiming Lu[a,b], Prashant Kumar Mishra[b], Timothy N. Hunter[b], Fan Yang[c], Zhouguang Lu[a], David Harbottle[b*] and Zhenghe Xu[a*]

[a]Department of Materials Science & Engineering, Southern University of Science and Technology, Shenzhen, 518055 Guangdong, P. R. China

[b]School of Chemical and Process Engineering, University of Leeds, Leeds, LS2 9JT, UK

[c]College of New Materials and New Energies, Shenzhen Technology University, Shenzhen 518118, P.R. China

## Abstract

Water is a valuable resource that is needed to sustain life, but is also essential in many engineering processes, which unavoidably leads to large volumes of water being contaminated. To achieve safe discharge and also recover valuable "pollutants", better performing sorbents are needed to rapidly and efficiently decontaminate water and generate minimal secondary wastes. Bio-sorbents derived from pomelo peel were functionalized with pyrrolic-N (BNC-5 electrode) and pyridinic-N (BNC-6 electrode) to enhance electroadsorption and selectivity of $Pb^{2+}$ and $Cu^{2+}$. The interaction between soft acid ions ($Pb^{2+}$) and soft base sites (pyrrolic-N) contributed to a strong chemisorption that elevated the electroadsorption capacity to ~2.0 mmol $g^{-1}$ for $Pb^{2+}$ at an applied voltage of 1.2 V. With fast removal kinetics (0.077 g $mg^{-1}$ $min^{-1}$ of $Pb^{2+}$), the BNC-5 sorbent exhibited comparable characteristics to other N-doped sorbents prepared using graphene. The large adsorption-desorption hysteresis of BNC-5 in responding to the applied electric voltage confirmed the chemisorption effect. The results showed only 32.4% of adsorbed ions being desorbed from the sorbent by reducing the applied voltage to 0 V, but almost complete desorption (98.5% of adsorbed ions) being achieved at –0.8 V. When operated in adsorption-desorption cycle mode, BNC-5 after ~400 cycles maintained a capacity retention ≥ 80%. After 400 cycles, the electrode capacity was almost fully restored (98.7%) by only mild chemical washing (0.1 M $HNO_3$) of the sorbent and the cycling performance maintained. The study demonstrated over 1200 cycles the robustness of sorbent and hence the potential to successfully convert waste into high-performance materials for large-scale remediation strategies using CDI.

**Keywords:** Capacitive deionization, bio-based sorbent, heavy metal ions, ion selectivity

## 1. Introduction

The World Health Organization (WHO) estimates that by 2025, half of the world's population will be living in water-stressed areas, and the crisis will continue to be exacerbated by higher levels of water pollution. With the fast growth of industries (mining, textiles, metal electroplating, steel and electronics) to meet the lifestyle expectations of a growing population, the release of heavy metals into the environment via discharge of industrial effluents has become inevitable, causing significant pollution of soils and groundwater [1]. According to a recent report from WHO, the presence of trace amounts of heavy metals in the air, drinking water and food can result in bioaccumulation and potentially cause serious health issues[2].

Although many decontamination methods have been designed and tested at scale, such as chemical precipitation [3], ion exchange [4], adsorption [5], membrane filtration [6] and osmosis [7], the practical use of such methods is often compromised by difficulties to selectively remove target (toxic) metal ions from concentrated industrial effluents, slow removal kinetics, limited ability to regenerate the sorbent material and high processing costs [8, 9]. Recently, capacitive deionization (CDI) has been highlighted as a method to overcome most limitations of existing methods with the focus being placed on improving the performance of the electrode sorbent materials [10, 11].

The CDI method operates by migrating ions in solution towards an electrode sorbent when a direct electric field is applied between oppositely polarized electrodes. The ions are captured by physical adsorption inside the pores of the electrode via the formation of an electric double layer (EDL), and can be released when the electric field is removed, making the CDI method a reversible process. To achieve good performance, electrode sorbents should possess high specific capacitance, low electrical resistivity, high specific surface area, good electrochemical stability and low fouling potential [10, 12]. Although many CDI electrode sorbents have been

tested to remove heavy metal ions, for example, amorphous carbon [13, 14], carbon nanotubes [15, 16], graphene [17, 18], and metal organic frameworks (MOFs) [19], the material costs and fabrication methods can prohibit their choice for large-scale decontamination strategies. More recently, researchers are exploring the performance of bio-based electrodes fabricated from agricultural or food wastes. Using a range of feedstocks including husk, palm leaflets, peels, straw and many others, electrodes for batteries, supercapacitors and CDI cells have been fabricated, showing promising results [20, 21]. This approach is exciting as the feedstocks are abundant, fabrication routes are relatively low cost, and the conversion of waste to high-performing materials accelerates the circular economy concept, helps reduce environmental pollution and addresses sustainability goals [22].

With a focus on CDI, Gaikwad et al. [23] prepared electrodes from rice husk to recover Cr(VI). The acid-treated activated carbon showed a moderate electrosorption capacity of 2.8 mg $g^{-1}$ from a feed concentration of 100 ppm at 1.2 V. Li et al. [12] converted watermelon into 3D-carbonaceous aerogels using a simple one-pot hydrothermal reaction, and with CDI at 1.2 V, showed a moderate recovery of $Cu^{2+}$ of ~20 mg $g^{-1}$ from an initial feed concentration of 50 mg $L^{-1}$ $CuCl_2$. Such studies showed the moderate performance of unmodified carbonaceous sorbents, which are inferior to the more commonly used sorbents. However, electrode performance can be significantly enhanced through chemical functionalization, with the chemistry tailored to increase selectivity and adsorption capacity of the target ion(s). For heavy metal ions removal, N- or S-containing groups are often favored due to the free non-bonding electron that can act as a Lewis base for the selective ion binding [24]. The approach of nitrogen functionalization to remove $Pb^{2+}$ and $Cu^{2+}$ from contaminated water has mostly been demonstrated for non-bio-based materials such as mesoporous carbon [25], activated carbon [26], carbon nanotubes [27], silica [28], MOFs [29] and graphene [17], but as shown in Table 1, the performance depends on several factors including the source of N-containing groups and

geometry of surface[30].

Zheng et al. [31] used dicyandiamide to form n-doped biomass-activated carbon (raw material – saw dust) prepared via ultrasonication and redox methods. The nitrogen content in the sample prepared via the redox method was higher, and formed additional n-functional groups of pyridinic-N-oxyde and R-C=NH, including pyridinic-N and pyrrolic-N that were also present in samples prepared using the ultrasonication method. However, the pore structure of samples prepared using the redox method was inferior to that prepared using the ultrasonication method, and the authors attributed the improved adsorption capacity of the sample using the redox method (Cu(II), $q_m \sim 15$ mg $g^{-1}$), as compared with all other samples, to pyridinium nitrogen and amine groups. Similar conclusions were made by Chen et al. [32] who complemented the deconvoluted XPS spectra with energetic molecular modelling (Atoms in Molecules) to show that anionic Cr(VI) is mostly adsorbed by protonated amine groups via electrostatic attraction. Ji et al. [17] prepared N-functionalized graphene and showed that pyridinic-N groups preferentially interacted with "hard" ions such as $Na^+$ and $H^+$, while pyrrolic-N groups interacted more strongly with "soft" ions such as $Pb^{2+}$. The adsorption capacity of $Pb^{2+}$ when combined with CDI was 481.5 mg $g^{-1}$ for pyrrolic-N modified graphene in contrast to 196.8 mg $g^{-1}$ for pyridinic-N modified graphene. The superior removal mechanism was due to Lewis acid-base interactions, where positively charged metal cations act as a Lewis acid while the electron donor -N groups act as a hard or soft Lewis base. According to the HSAB (Hard-Soft Acids and Bases) principle, the most favorable interactions would be between hard acids ($H^+$ and $Na^+$) and hard bases (pyridinic-N) or soft acids ($Pb^{2+}$) and soft bases (pyrrolic-N), leading to the formation of stable metal-ligand bonds [33].

Table 1 summarizes the performance characteristics of carbon-based sorbents to remove $Cu^{2+}$ and $Pb^{2+}$ from contaminated water when combined with CDI. The table is sub-divided into

those materials that are N-functionalized, and those which are not. The better performing sorbents are the N-functionalized materials, and the sorbent substrate is either graphene nanosheets or graphene aerogel, highlighting no exploration of other substrate materials, particularly bio-derived substrates.

**Table 1.** Carbon-based sorbents used with CDI to remove $Cu^{2+}$ and $Pb^{2+}$ from contaminated water.

| Materials | Methods | Surface area ($m^2 g^{-1}$) | Pore size (nm) | Adsorbate | Electroadsoprtion Capacity (mg $g^{-1}$) | Removal efficiency (%) | Voltage (V) | Ref. |
|---|---|---|---|---|---|---|---|---|
| CAs/MO | Hydrothermal | 262.6 | 5.4 | $Cu^{2+}$ | 57.1 | 69.2 | 1.2 | [12] |
| Activated carbon | - | 964 | 2.1 | $Cu^{2+}$ | 24.6 | - | 0.8 | [34] |
| $MnO_2$/CF | Electrodeposition | 2 | 2 | $Cu^{2+}$ | 172.9 | 90 | 0.8 | [35] |
| Activated carbon | Heating and activation | 1162 | 1-4.5 | $Cu^{2+}$ | 77.8 | - | 1.2 | [36] |
| rGO/NCDs | Hydrothermal | 347.6 | 3.8 | $Pb^{2+}$ | 19.3 | ~55% | 1.0 | [37] |
| Graphene-EDTA | Hydrolysis/ grafting | - | - | $Pb^{2+}$ | - | 99.9 | 1.4 | [38] |
| Activated carbon cloth | - | - | - | $Pb^{2+}$ | - | 81 | 1.2 | [39] |
| CNTs | Air-plasma treated | 106 | - | $Pb^{2+}$ | 2.4 | - | 1 | [16] |
| **N-functionalized Carbon** | | | | | | | | |
| N-doped graphene nanosheets | Calcination | 695 | 3.5 | $Pb^{2+}$ | 521 | > 90 | 1.2 | [8] |
| N-doped 3D graphene aerogel | Hydrothermal | 434 | - | $Cu^{2+}$ | 119.9 | ~55 | 0.3 | [18] |
| N-doped 3D graphene aerogel | Hydrothermal | 434 | 4.86 | $Pb^{2+}$ | 650.4 | 75 | 0.3 | [40] |
| N-doped graphene | Hydrothermal | 198 | 1-6 | $Pb^{2+}$ | 481.5 | ~100 | 1.2 | [17] |
| Pyrrolic-N Pyridinic-N | Hydrothermal | 268 | 1-6 | $Pb^{2+}$ | 196.8 | ~100 | 1.2 | |

Nomenclature: CNTs – carbon nanotubes; CAs/MO – carbon aerogel/metal oxide; $MnO_2$/CF – $MnO_2$/carbon fiber; Graphene-EDTA – Graphene- Ethylene Diamine Tetraacetic Acid; rGO/NCDs – reduced graphene oxide/nitrogen-doped carbon quantum dots.

In the current study, CDI electrodes (Fig. 1d) were fabricated from waste pomelo peel. Pomelo is a citrus fruit that is widely grown in Asia, Africa and Australia. While producing delicious juice, pomelo generates a significant amount waste (peel) that is often sent to landfill [41]. Studies have begun to demonstrate routes to convert waste pomelo peel to the functionalized sorbent material to enhance the removal and selectivity of organic species such as methylene blue [42], methyl orange [43, 44], Rhodamine B and 6G [43] and ketamine [45] (an emerging

contaminant) from the contaminated water. Tasaso [46] was among the first who studied the use of pomelo peel to remove heavy metal ions ($Cu^{2+}$) from contaminated water. In this study, the adsorbent was not chemically or thermally modified and thus the adsorption capacity remained low at ~20 mg $g^{-1}$. Since then further advancements in the preparation of sorbents from pomelo peel have been made, including for example: i) magnetic pomelo peel biochar with removal capacities of 205 mg $g^{-1}$ and 82 mg $g^{-1}$ for Pb(II) and Cu(II), respectively [47]; ii) pomelo peel carbonized with phosphoric acid to adsorb Ag(I) (adsorption capacity = 137.4 mg $g^{-1}$) and Pb(II) (adsorption capacity = 88.7 mg $g^{-1}$) [48]; and iii) pomelo peel carbonized with ammonium dihydrogen phosphate and further modified using potassium bicarbonate to prepare an electrode for deionization of salt solutions, demonstrating a salt adsorption capacity of < 20 mg $g^{-1}$ at 1.4 V in a 500 mg $L^{-1}$ NaCl solution flowing at 40 mL $min^{-1}$ [49]. The electrodes in the current study were fabricated using the pomelo peel char carbonized with $KHCO_3$ activation (Fig. 1b), followed by functionalization with pyrrolic-N groups (BNC-5) or pyridinic-N groups (BNC-6) to enhance the selectivity and removal of $Pb^{2+}$ and $Cu^{2+}$ from contaminated water (see Fig. 1a). When combined with CDI (Fig. 1c), both the adsorption capacity and removal kinetics were anticipated to be substantially enhanced due to the combined effect of physisorption and chemisorption. The dominant removal mechanism was determined from the adsorption/desorption hysteresis of the as-prepared electrodes in response to the applied voltage. More importantly, we demonstrated successful removal (desorption) of the adsorbed metal ions from the sorbent by applying a mild reversing voltage of -0.8 V to regenerate the electrode, thus extending the lifetime of the sorbent and avoiding the generation of secondary wastes as often encountered by chemical (acid) stripping and regeneration. The study has compared the long-term cycling performance of the fabricated electrode against activated carbon, and demonstrated near complete recovery of sorbent performance by intermittent (every several hundred cycles) weak chemical washing.

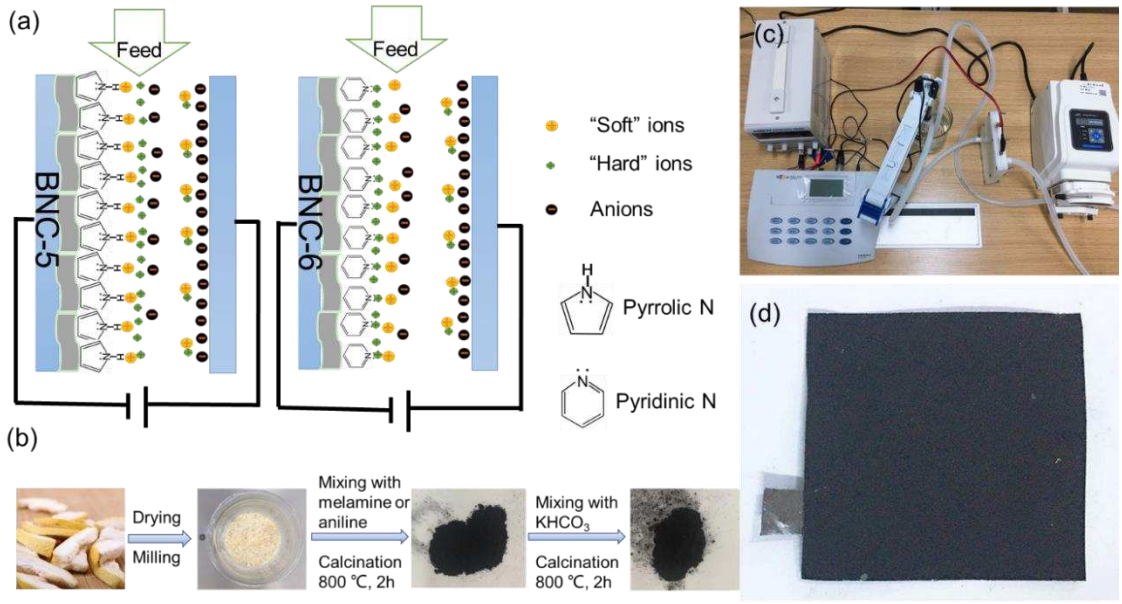


**Figure 1.** (a) Illustration of selective adsorption of metal ions by BNC-5 and BNC-6; (b) step-by-step fabrication method to form BNC-5 and BNC-6; (c) photograph of the CDI set up (including the CDI cell, direct power source, conductivity meter, peristaltic pump and feed beaker); and (d) photograph of the as-prepared CDI electrode.

## 2. Materials and Methods

**2.1 Material Synthesis and Characterization:** As shown in Fig. 1b, the biomass derived carbon (BC) and N-doped BC (BNC-5 for five-ring pyrrolic-N and BNC-6 for six-ring pyridinic-N functionalization) were prepared by a facile two-step calcination process. The method was slightly adapted from previous studies for the preparation of carbon-derived from pomelo peel [17, 50]. First 5 g of fresh pomelo peels were dried at 80 °C for 24 h and milled into powder using an agate mortar. Afterwards, the obtained powder was mixed with either melamine (pyrrolic-N source for BNC-5) or aniline (pyridinic-N source for BNC-6) at a mass ratio of 1:1 and heated in a tube furnace at 800 °C for 2 h under 1 L $min^{-1}$ nitrogen flow. The reaction time was fixed at 2 h since doubling the reaction time (4 h) led to only a marginal increase (~10%) in the nitrogen content (see Fig. S4a), and would compromise the ability to

complete the reaction steps in a single day. The sample was allowed to cool naturally to room temperature before the activating agent, $KHCO_3$, was added to the calcined carbonized powder at a mass ratio of 1:1 and then further calcined at 800 °C for 2 h under 1 L $min^{-1}$ nitrogen flow. The powder obtained was cooled at room temperature before washing the sample with 2 M HCl and then an excess of distilled water until the supernatant pH was 7. Finally, the sample was dried in an oven at 80 °C for 24 h. For comparison, BC was prepared using the same procedure without adding melamine or aniline. A commercially available activated carbon (AC) from Sigma Aldrich was also used for comparison.

**Transmission electron microscope:** Transmission electron microscopy (TEM) and high-resolution TEM (HR-TEM) images of the prepared samples were collected using a FEI Titan Themis Cubed 300 microscope (Thermo Fisher Scientific) at 300 kV acceleration voltage. The samples were dispersed (ppm level) in ethanol by ultrasonication for 5 min and then one drop of the dilute suspension was deposited onto an amorphous carbon film on a copper grid (Agar Scientific Ltd.) and dried under an infrared lamp for analysis.

**Scanning electron microscope:** A TM3030Plus scanning electron microscope (SEM) (Hitachi) with energy dispersive X-ray spectroscopy (EDX, Oxford Instruments, X-stream-2) was used to determine morphology and elemental composition of the sample. The acceleration voltage was set at 10 kV with a working distance of 8 mm. Samples were dispersed in ethanol and one drop of the sample was placed on a single-crystal silicon wafer for characterization.

**Nitrogen adsorption/desorption analysis:** The nitrogen adsorption/desorption isotherms were obtained using a TriStar 3000 analyzer (Micrometrics, UK) after degassing the sample at 200 °C for 6 h. The specific surface area of each sample was determined by the Brunauer–Emmett–Teller (BET) method and the pore size distribution was calculated from the branches of the

nitrogen adsorption isotherm via the Barrett–Joyner–Halenda (BJH) model.

**X-ray photoelectron spectroscopy:** X-ray photoelectron spectroscopy (XPS) was used to analyze the surface chemical state of each sample. The XPS spectrum was obtained using a VG Multilab 2000 apparatus with a monochromated Al K-alpha X-ray source of 1486.6 eV (Thermo Fisher, Escalab 250Xi, USA). Charge build-up on the sample during the measurement was compensated by an electron/ion gun. BC, BNC-5 or BNC-6 powder was placed in the measurement chamber and the vacuum maintained at $<10^{-7}$ Pa. All spectra were calibrated against the C 1s peak (285 eV) and deconvoluted with the Avantage software using the Powell fitting algorithm with Gauss-Lorentz mix product and 0.0001 convergence value.

**2.2 Electrode Preparation and Metal Ion Adsorption:** The CDI working electrode was prepared by mixing the active material (BNC-5, BNC-6 or BC), super P (Kejing Ltd.) and polyvinylidene fluoride (PVDF, Sigma Aldrich) at a mass ratio of 8:1:1 in N-methyl-pyrrolidone (NMP) under magnetic stirring for 12 h. The prepared slurry was then spread onto a 10-μm thick graphite paper (Jilong Special carbon) using a film applicator machine (MSK-AFA-ES200, Kejing Ltd.) with a gap spacing of 200 μm and a coater speed of 3 mm/s. The sample was then dried at 80 °C for 12 h in a vacuum oven. Finally, the electrodes were cut to 80 × 80 mm (Fig. 1d) such that the dry mass of active material was ∼200 mg. To ensure consistency between different electrodes, only electrodes with a total mass within 5% of the initially prepared electrode mass were used in the study.

The recoveries of $Cu^{2+}$ and $Pb^{2+}$ by the fabricated and standard materials was assessed using a continuous CDI (Fig. 1c) which comprised of a custom-built CDI cell, power source (RXN-605D, Zhaoxin), peristaltic pump (BT100-2J, Lange), conductivity meter (Type 308A, Leici Company) and 500 mL feed and discharge beakers. The flow geometry of the CDI cell included

one working electrode and one counter electrode (graphite paper, Jilong Special Carbon ) separated by a 1-mm thick silicon rubber seal. For each CDI test, 200 mL of contaminated water was cycled through the CDI cell at 20 mL/min while applying a direct voltage of either 0 V (open circuit) or 1.2 V (closed circuit). The concentration of $Cu(NO_3)_2$ in aqueous solution was varied from 0.31 to 3.15 mmol $L^{-1}$ and for $Pb(NO_3)_2$ the concentration was varied from 0.10 to 0.97 mmol $L^{-1}$, while the solution pH was kept constant at 5.0 ± 0.1. An atomic adsorption spectrophotometer (AAS, 200 Series AA, Agilent Technologies) was used to determine the ion concentration remaining in solution following each test. The adsorption capacity of the test material was calculated by:

$$q = \frac{(C_0 - C_e)V}{m} \quad (1)$$

where $C_0$ and $C_e$ (mmol $L^{-1}$) represent the initial and equilibrium ion concentrations, respectively, $V$ (mL) is the test solution volume and $m$ (mg) is the mass of the active material (not including the mass of binder and conductive agent).

**Adsorption kinetics:** The different sorbents were evaluated using the CDI setup operating with an applied voltage of 0 V or 1.2 V as 0.79 mmol $L^{-1}$ $Cu^{2+}$ or 0.24 mmol $L^{-1}$ $Pb^{2+}$ ($C_0$ – initial concentration) test solution was cycled through the CDI electrode at 20 mL/min. The concentration ($C_t$ – time dependent concentration) of $Cu^{2+}$ or $Pb^{2+}$ was measured by AAS by sampling from the 200 mL test solution at 5, 15, 30, 45, 60, 90 and 120 min.

**Competitive adsorption:** The adsorption of $Cu^{2+}$ or $Pb^{2+}$ from a complex mixture of competing ions ($Na^+$, $K^+$ and $Ca^{2+}$) was studied using the CDI setup. All nitrate salts were purchased from Aladdin Chemicals (China) and used without further purification. Test solutions were prepared

to 200 mL and the concentrations of the competing ions were varied from 1.0 mmol $L^{-1}$ to 10.0 mmol $L^{-1}$. The target ion concentration was fixed at 0.79 mmol $L^{-1}$ for $Cu^{2+}$ and 0.24 mmol $L^{-1}$ for $Pb^{2+}$. The test solutions were circulated through the CDI cell at a constant volumetric flow rate of 20 mL/min for 30 min with a fixed applied voltage of 1.2 V.

**Electrode durability:** The fluid volume at breakthrough of BNC-5 was measured against an upper limit concentration of 1 ppm (equal to 0.016 mmol $L^{-1}$ for $Cu^{2+}$ or $4.8\times10^{-3}$ mmol $L^{-1}$ for $Pb^{2+}$), which is considered as the maximum discharge concentration for copper and lead (GB 8978-1996)[51, 52]. For these tests, it should be noted that the electrode thickness was increased such that the electrode mass was 500 mg. The CDI voltage was fixed at 1.2 V while the test solution of 0.31 mmol $L^{-1}$ $Cu^{2+}$ or 0.1 mmol $L^{-1}$ $Pb^{2+}$ was pumped at a flow rate of 1 mL/min for a single pass through the CDI cell. The initial volume of the test fluid was 400 mL and the test was repeated several times by increasing the test fluid volume by 50 mL each time until the breakthrough concentration (0.016 mmol $L^{-1}$ for $Cu^{2+}$ or $4.8\times10^{-3}$ mmol $L^{-1}$ for $Pb^{2+}$) was exceeded.

The ability to regenerate electrodes (milled-AC, BC, BNC-5 and BNC-6) was assessed by cycling the CDI applied voltage between 1.2 V (adsorption) and 0 V (desorption). Test solutions of either 0.79 mmol $L^{-1}$ $Cu^{2+}$ or 0.24 mmol $L^{-1}$ $Pb^{2+}$ were cycled around the CDI cell at 20 mL/min. For each adsorption and desorption step, the applied voltage was held constant for 10 min (20 min per cycle). After 20 cycles the test fluid was sampled to measure the amount of $Cu^{2+}$ or $Pb^{2+}$ retained by the electrode. The capacity retention is given by $q_x/q_{1st}$; where $q_x$ is the adsorption capacity at $x$ cycles, and $q_{1st}$ is the adsorption capacity after the first cycle. For certain tests, when the capacity retention dropped to 80%, the electrodes were removed from the CDI cell and were chemically regenerated by soaking in 0.1 M $HNO_3$ for 30 min.

The effect of applied voltage on the sorption capacity of the fabricated electrodes was studied from −0.8 V to 1.6 V. Using test solutions of 0.79 mmol $L^{-1}$ $Cu^{2+}$ or 0.24 mmol $L^{-1}$ $Pb^{2+}$, 200 mL of the test fluid was cycled around the CDI cell at 20 mL/min for 30 min. To study adsorption, the applied voltage was varied between 0 V and 1.6 V. To study desorption, the CDI electrode was first operated with an applied voltage of 1.6 V for 30 min and then the applied voltage was lowered to the new voltage and held for a further 30 min. To avoid issues of possible ion retention, new electrodes and fresh test solutions were used for each experiment.

## 3. Results and Discussion

### 3.1 Structure Characterization of Sorbent

SEM images and elemental mapping via Energy-dispersive X-ray spectroscopy (EDS) of the fabricated samples (BC, BNC-5 and BNC-6) are shown in Fig. 2. The top row of images shows the samples to have a flake-like morphology with visible surface roughness. As measured by dynamic light scattering, the mean particle sizes were 28.3, 25.6 and 30.8 μm for BC, BNC-5 and BNC-6, with a particle size distribution between 5.0 – 42.1 μm (BC), 5.6 – 45.3 μm (BNC-5), and 4.1 – 43.5 μm (BNC-6), respectively. The bottom row of images shows the nitrogen EDS maps with the corresponding SEM images shown in the inset. The presence and uniform distribution of nitrogen in BNC-5 and BNC-6 confirms the successful functionalization of the carbonized material, providing an abundance of adsorption sites for the heavy metal ions and increasing the electrical conductivity of the material [8, 17]. The fourth test sample, milled-AC, is shown in Fig. S1 for comparison. As observed in SEM micrographs, the particles do not show any flake-like morphology with a mean particle size of 500 μm and particle size distribution between 300 – 1500 μm.

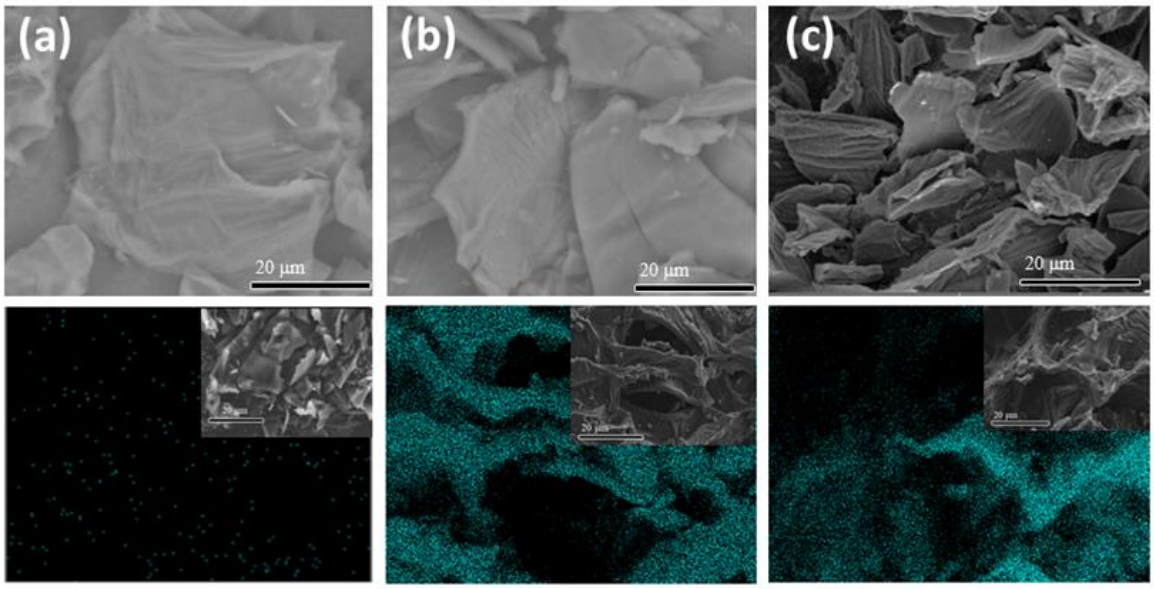


**Figure 2.** SEM images (top) and nitrogen EDS mapping (bottom) of (a) BC, (b) BNC-5 and (c) BNC-6 with insets showing the corresponding SEM images.

With the limited resolution of SEM, the three fabricated samples were also analyzed using TEM to determine if the samples modified by pyrrolic-N and pyridinic-N subtly changed their morphology and pore structure. The three samples imaged at increasing magnification (Fig. 3) did not show any differences in the material macro- and meso-structure, thus confirming no visible effect of the N-doping on the sorbent morphology. The flake-like morphology observed by TEM confirmed the material to be composed of thin sheets which increase the surface area, thus creating more adsorption sites for the heavy metal ions. For all three samples, a mesoporous structure was observed which is highlighted by the arrows and circles in the high resolution TEM (HR-TEM) images (Fig. 3). These mesopores (appearing as white dots) were evenly distributed throughout the sample, with the mesopores being generated during the activation by $KHCO_3$ at high temperatures. This modification was added to improve both the water permeation and adsorption capacity of the materials[53]. The HR-TEM images did not reveal any crystallinity in BC, BNC-5 and BNC-6, and this was also confirmed by the lack of any diffraction patterns when measured by selected area electron diffraction (SAED), see Fig.

S2. As such, the three fabricated sorbents are characterized as amorphous solids.

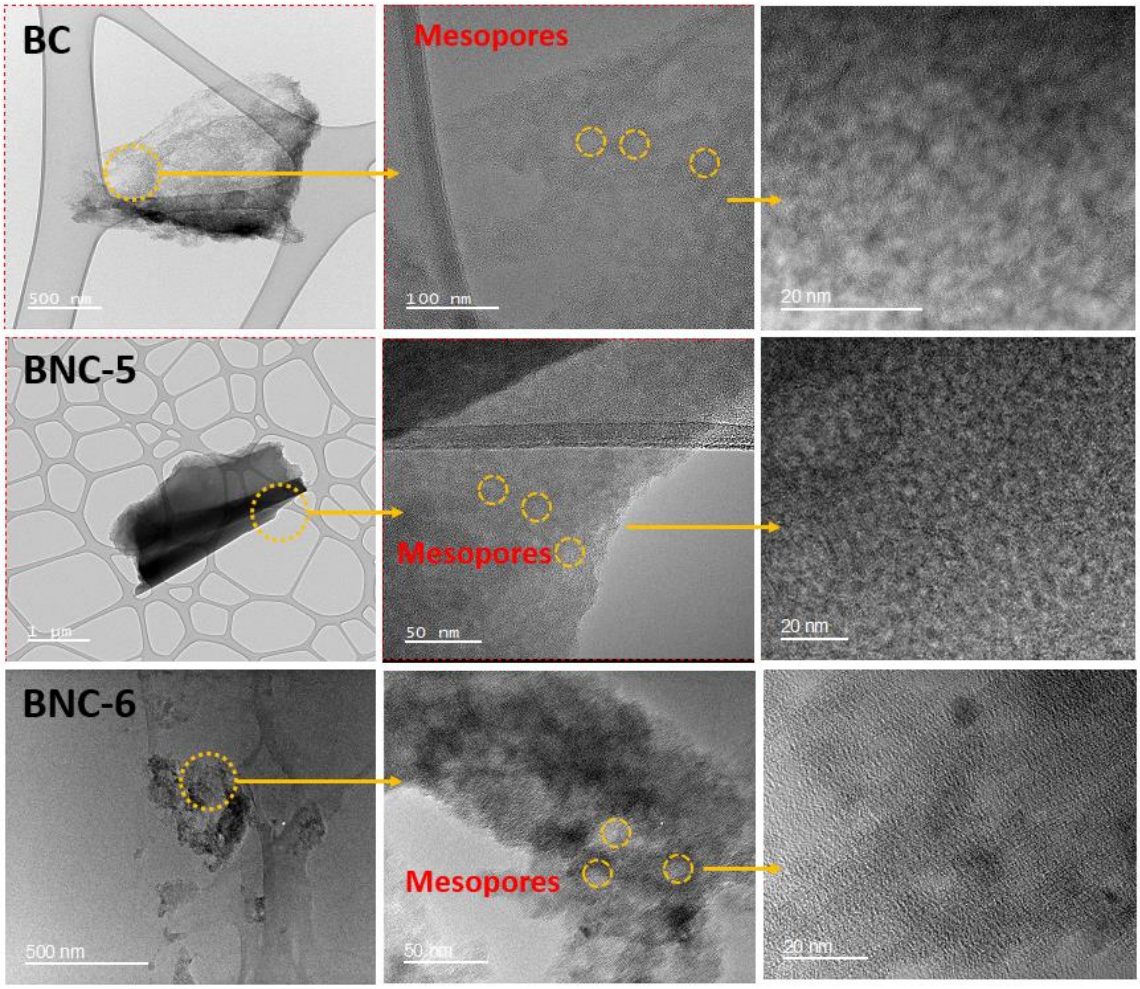


**Figure 3.** TEM and HR-TEM images of BC, BNC-5 and BNC-6. The dashed circles highlight the mesopores within the sorbent structure.

### 3.2 BET Surface Area Analysis

The nitrogen adsorption/desorption isotherms and pore size distribution of all prepared samples and milled-AC are shown in Fig. 4a and 4b. The specific surface area (SSA) and mean pore size for each sorbent is summarized in Table 2. All fabricated sorbents exhibited similar properties, but were significantly different to milled-AC which was characterized by a much lower SSA and a mean pore size of 1.6 nm, which is attributed to the higher proportion of micropores. Based on the understanding that micropores are less than 2 nm and mesopores

between 2 and 50 nm[54], the fabricated sorbents were found to have a higher proportion of mesopores which were created by the $KHCO_3$ activation process. Electrosorption in mesopores is not significantly limited by overlapping electrical double layers (EDL)[55], thus the sorption capacity can be higher. Moreover, the increased ion diffusion and enhanced permeability to water in mesopores, all contribute to increasing the number of accessible surface sites for ion adsorption[56]. The water droplet contact angle ($\theta$) measurements (Fig. S3) revealed a similar wettability (~25°) for BC, BNC-5 and BNC-6 as anticipated, while milled-AC was found to be more hydrophobic with $\theta$ = 87°.

**Table 2.** Physical properties of the sorbent materials.

| Sample | Surface area ($m^2\ g^{-1}$) | Mean pore size (nm) | Proportion (%) | |
|---|---|---|---|---|
| | | | micropore | mesopore |
| **AC** | 752.5 | 1.6 | 76.2 | 23.8 |
| **BC** | 1431.5 | 2.6 | 16.3 | 83.7 |
| **BNC-5** | 1434.2 | 2.9 | 14.4 | 85.6 |
| **BNC-6** | 1461.2 | 2.7 | 14.9 | 85.1 |

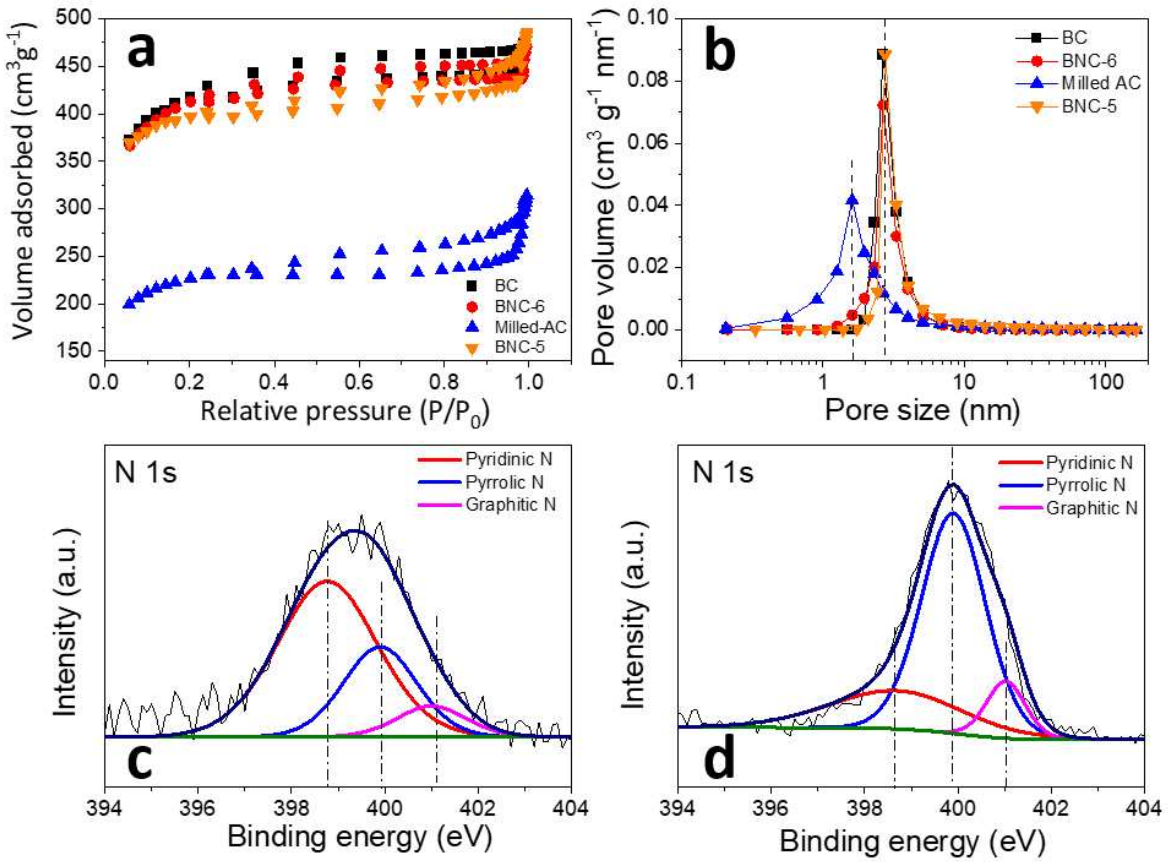


**Figure 4.** Nitrogen adsorption/desorption isotherms (a) and pore size distributions (b) of BC, BNC-5, BNC-6 and milled-AC. XPS N 1s spectra and corresponding fittings are given in (c) and (d) for BNC-5 and BNC-6, respectively.

### 3.3 Chemical Composition of Sorbent

X-ray photoelectron spectroscopy (XPS) was used to confirm the successful N-functionalization of BNC-5 and BNC-6 sorbents. The survey spectra of all 3 samples (BC, BNC-5 and BNC-6) including peaks of C 1s and O 1s are provided in the Supporting Information, see Fig. S4b and S5. The relative N-content in BNC-5 and BNC-6 was 3.14 at% and 2.96 at%, respectively. The N 1s core level spectra of BNC-5 and BNC-6 are shown in Fig. 4c and 4d, with the spectra further deconvoluted into three peaks at 398.6, 399.9 and 401.1 eV, which correspond to the pyridinic-N, pyrrolic-N and graphitic-N, respectively[57]. Curve area analysis revealed the contents of pyridinic-N, pyrrolic-N and graphitic-N in BNC-5 to be 23.8 %,

65.8 % and 10.4 %, respectively, in contrast to 63.9 % (pyridinic-N), 27.3 % (pyrrolic-N) and 8.8 % (graphitic-N) for BNC-6. These results confirm the successful protocol of surface functionalization of the amorphous carbon with pyrrolic-N being prevalent in BNC-5 and pyridinic-N prevalent in BNC-6, as desired. A full quantitative analysis of the XPS spectra for BC, BNC-5 and BNC-6 are provided in the Supplementary Information, Table S1.

### 3.4 CDI Measurements

The performance of the fabricated (BC, BNC-5, BNC-6) and standard (milled-AC) sorbents to remove heavy metal ions from contaminated water was assessed in open circuit (0 V) and closed circuit (1.2 V) modes of CDI, as shown in Fig. 5. The 0 V data was fitted using the Langmuir adsorption model, $Q_e = \frac{Q_0 K_L C_e}{1+K_L C_e}$, with the fitting parameters determined by transforming the equation into its linear form[58]:

$$\frac{1}{Q_e} = \frac{1}{Q_0} + \frac{1}{Q_0 K_L C_e} \quad (2)$$

where $C_e$ (mmol $L^{-1}$) and $Q_e$ (mmol $g^{-1}$) are the equilibrium concentrations of adsorbate in the liquid and solid phase, $K_L$ represents the Langmuir constant relating to the affinity coefficient between the ions and the binding sites (L $mmol^{-1}$), and $Q_o$ is the theoretical maximum adsorption capacity (mmol $g^{-1}$). Similar fittings of Langmuir isotherms were not made for data obtained at 1.2 V due to the strong electrosorption effect in an applied electrical fields.

The adsorption isotherms were well-described by the Langmuir model (Fig. 5a and 5b) and the fitting parameters are summarized in Table S2. In the open circuit mode (0 V), the adsorption performance improved in the following order, milled-AC < BC < BNC-6 < BNC-5, with the theoretical maximum adsorption capacity of BNC-5 for $Pb^{2+}$ and $Cu^{2+}$ equal to 1.05 and 0.70

mmol $g^{-1}$. While the poor performance of milled-AC is attributed to its physical properties (low specific surface area and small volume of micropores), the performance variation between BC, BNC-5 and BNC-6 appears to be more influenced by the chemistry of the sorbents. As discussed by Ji et al.[17], sorbents functionalized with pyridinic-N and pyrrolic-N enhance the basic nature of the carbon material, with pyridinic-N acting as a harder base than pyrrolic-N. From the study of Sigel et al.[59], $Cu^{2+}$ is described as being neither a hard or soft ion but a borderline ion, while $Pb^{2+}$ is a soft ion. The adsorption capacity of BNC-5 for $Pb^{2+}$ is anticipated to be higher than $Cu^{2+}$, confirming the preferential interaction between BNC-5 and soft ions. Nevertheless, the surface functionalization of pyrrolic-N on BNC-6 did enhance adsorption of $Cu^{2+}$ as compared with the case for BC.

Figures 5c and 5d compare adsorption isotherms for the different materials operating in closed circuit mode (1.2 V) of CDI. Similar to the open circuit mode of CDI, the same trend in material performance was observed. The absolute changes in ion adsorption from open to closed circuit mode of CDI were greater for the N-functionalized sorbents. For BNC-5 and BNC-6, the increased adsorption capacity more than doubled when increasing the applied voltage from 0 V to 1.2 V. BNC-5 exhibits the highest electroadsorption capacities of 1.46 mmol $g^{-1}$ (93.3 mg $g^{-1}$) for $Cu^{2+}$ and 2.05 mmol $g^{-1}$ (424.7 mg $g^{-1}$) for $Pb^{2+}$, comparable to electroadsorption capacities of graphene-based materials, see Table 1. This enhancement cannot only be attributed to the effect of electroadsorption (EDL adsorption by electrostatic attraction), since there remains significant differences between adsorption capacities among the three fabricated materials. The chemical modification appears to result in a synergistic effect arising from activation of chemical sites by the applied electrical field. Early studies have shown that N-doping improved the electrical conductivity of carbon-based sorbents in addition to increasing ion diffusion through N-induced defects that lowers the activation energy of adsorption [60, 61]. It is hypothesized the strong electrostatic attraction of ions into the Stern layer could partially

dehydrate metal ions to lower the binding energy of N with dehydrated ions and to increase the number of accessible binding sites.

For the best performing sorbent, BNC-5, the electroadsorption capacities for $Cu^{2+}$ and $Pb^{2+}$ are comparable to other graphene-based substrates that were N-functionalized and used with CDI to recover either $Cu^{2+}$ or $Pb^{2+}$. Being comparable in performance is encouraging to continue to develop bio-based sorbents that could replace the more costly materials that are often considered for CDI. It would also promote greater sustainability and contribute to the emerging circular bio-economy.

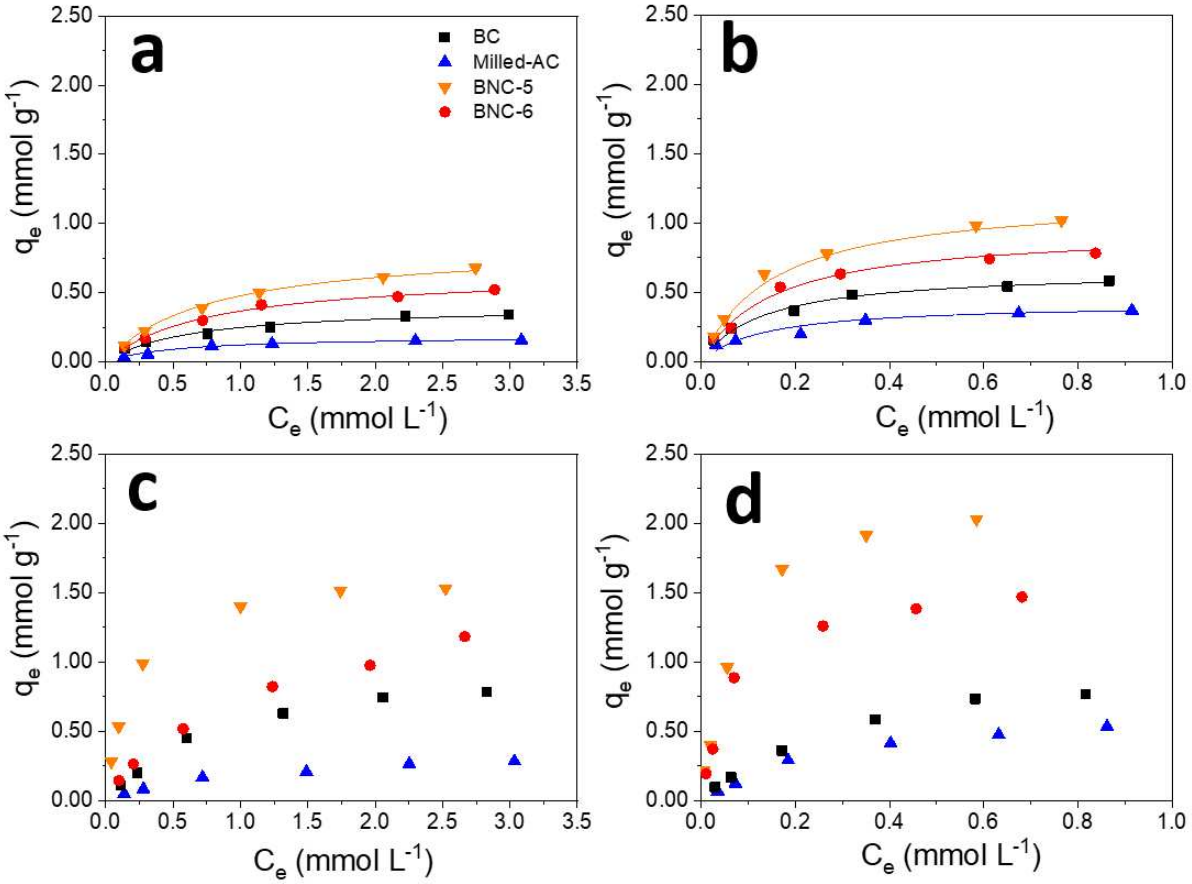


**Figure 5.** Adsorption isotherms of milled-AC, BC, BNC-5 and BNC-6 for (a) $Cu^{2+}$ and (b) $Pb^{2+}$ removal at 0 V (open circuit mode of CDI) and (c) $Cu^{2+}$ and (d) $Pb^{2+}$ removal at 1.2 V (closed circuit mode of CDI). The initial concentration of $Cu^{2+}$ or $Pb^{2+}$ was increased from 0.31 to 3.15

and 0.10 to 0.97 mmol $L^{-1}$, respectively. Solid lines represent Langmuir isotherm fits.

The adsorption kinetics were measured in both open (0 V, Fig. 6a and 6c) and closed (1.2 V, Fig. 6b and 6d) circuit modes of CDI. The experimental data was fitted to the pseudo-second order rate equation (PSORE)[58]:

$$\frac{t}{Qt} = \frac{1}{k_2 Q_e^2} + \frac{t}{Q_e} \tag{3}$$

where $Q_t$ (mmol $g^{-1}$) and $Q_e$ (mmol $g^{-1}$) are the quantities of adsorbed ions at time t and at equilibrium, and $k_2$ (g $mg^{-1}$ $min^{-1}$) is the adsorption rate constant.

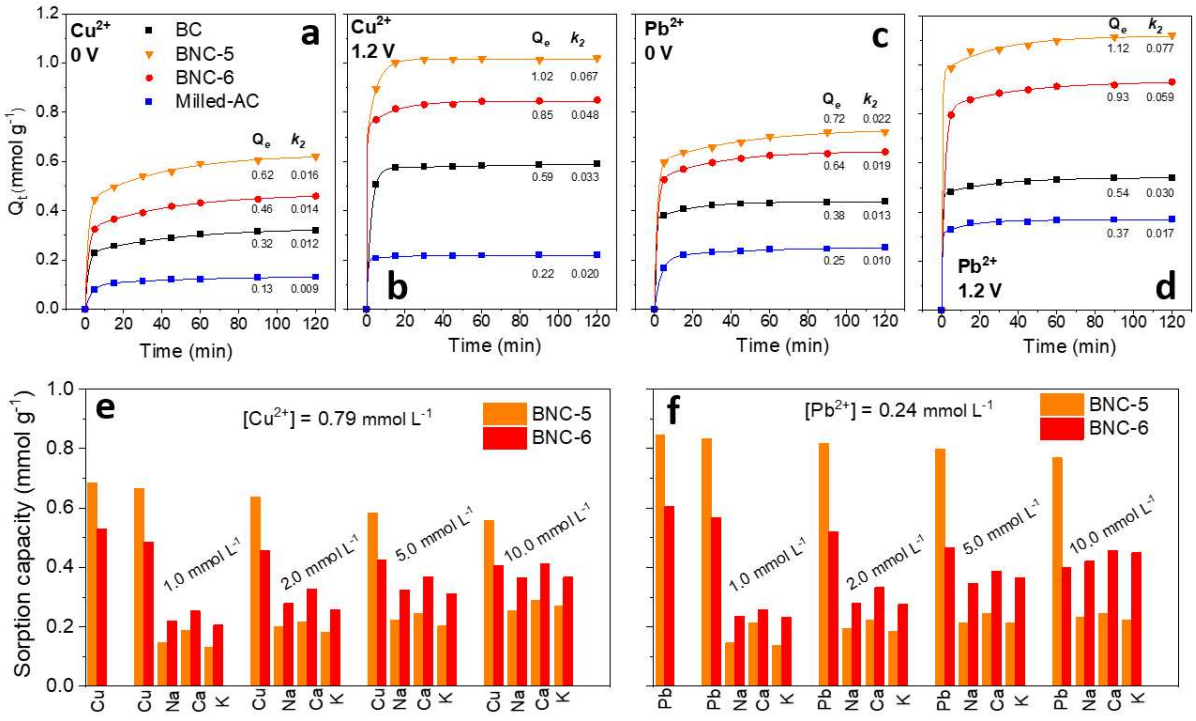


**Figure 6.** Adsorption kinetics for $Cu^{2+}$ (a, b) and $Pb^{2+}$ (c, d) by milled-AC, BC, BNC-5 and BNC-6 operated in (a, c) open circuit (0 V) and (b, d) closed circuit (1.2 V) modes of CDI; Competitive adsorption of (e) $Cu^{2+}$ and (f) $Pb^{2+}$ from mixed metal ion solutions containing $K^+$, $Na^+$ and $Ca^{2+}$. Unless otherwise stated, the initial concentration was 0.79 mmol $L^{-1}$ $Cu(NO_3)_2$ or 0.24 mmol $L^{-1}$ $Pb(NO_3)_2$.

The linearized form of the kinetic data, $t/Q_t$ vs. t is shown in Fig. S6 of the Supporting Information. The PSORE fits provided excellent agreement to the data, with $R^2$ coefficients > 0.99 (Table S2). For both open and closed circuit modes of CDI, the removal of $Cu^{2+}$ or $Pb^{2+}$ from contaminated water was found to mostly occur within the first 10 min of operation. For example, in the closed circuit mode of CDI, 90% of $Pb^{2+}$ was removed by BNC-5 in 10 min, in comparison to 84% by BNC-6. When comparing the adsorption rate constants, $k_2$ (g $mg^{-1}$ $min^{-1}$), applying 1.2 V in the closed circuit mode of CDI at least doubled the adsorption rate constant for BC, while for BNC-5 and BNC-6, an almost four-fold increase in $k_2$ was seen for both ion-types. In the removal of $Pb^{2+}$ by BNC-5, $k_2$ increased from 0.022 g $mg^{-1}$ $min^{-1}$ (0 V) to 0.077 g $mg^{-1}$ $min^{-1}$ (1.2 V), see Table S2 for all PSORE fitting parameter values. With no applied voltage (Fig. 6a and 6c), there was slight enhancement in the adsorption rate of $Pb^{2+}$ by BNC-5 and BNC-6 compared to $Cu^{2+}$, and the absolute difference was further increased when the CDI was operated with 1.2 V.

Figures 6e and 6f show the influence of competing ions when removing $Cu^{2+}$ or $Pb^{2+}$ using BNC-5 and BNC-6 in the closed circuit mode of CDI. When increasing the concentration of competing ions ($Na^+$, $Ca^{2+}$ and $K^+$) from 0 to 10 mmol $L^{-1}$ (per ion-type), the adsorption capacity of BNC-5 decreased by 18.8% and 9.4% for $Cu^{2+}$ and $Pb^{2+}$. For BNC-6, the adsorption capacity decreased by 24.5% and 29.4% for $Cu^{2+}$ and $Pb^{2+}$ over the same concentration range of competing ions. The interaction (binding) of BNC-5 with $Pb^{2+}$ is shown to be the most selective, for example, the selectivity ratio of $Pb^{2+}$ to $Na^+$ for BNC-5 was found to range from 6.1 to 3.6 for competing ion concentrations of 1 to 10 mmol $L^{-1}$, thus validating the principle of the N-doped modification. Moreover, the poorer selectivity of BNC-6 can be attributed to the preferred binding of the hard base sites with hard acid ions ($Na^+$, $K^+$ and $Ca^{2+}$).

The potential of BNC-5 to treat contaminated water in a single-pass through the CDI cell (1 mL/min) was studied to determine the volume of water at breakthrough, i.e. when the discharge concentration exceeded 0.016 mmol $L^{-1}$ for $Cu^{2+}$ or $4.8\times10^{-3}$ mmol $L^{-1}$ for $Pb^{2+}$ (equivalent to 1 ppm). From an initial concentration of 0.31 mmol $L^{-1}$ for $Cu^{2+}$ and 0.1 mmol $L^{-1}$ for $Pb^{2+}$, the sorbent BNC-5 was able to treat 770 mL of $Cu^{2+}$ and 890 mL of $Pb^{2+}$ contaminated water before breakthrough (Fig. S7). Based on the mass of sorbent used, this would equate to treating 1.54 L ($Cu^{2+}$) and 1.78 L ($Pb^{2+}$) of contaminated water per gram of sorbent.

A unique feature of the CDI approach is the ability to desorb ions without the need for frequent chemical washing. The sorbent material has the potential to be reused hundreds of times without significant deterioration in performance. Furthermore, through electrode cycling, the adsorbed metal ions can be discharged from the electrode as a concentrated waste solution (i.e. small volume of discharge water), thus reducing the difficulties in further treatment and storage. The durability of the three fabricated sorbents (BC, BNC-5 and BNC-6) were first assessed by cycling the applied voltage of the CDI between +1.2 V for adsorption and -0.8 V (where almost full ion discharge is achieved, see Figs. 7c and 7d) for desorption (stripping). A comparison of CDI cyclic performance for $Cu^{2+}$ and $Pb^{2+}$ removal is shown in Fig. S8, and confirms the excellent stability of the three sorbents without any apparent (within measurement error) reduction in the capacity retention over 300 cycles.

A much longer CDI durability test was conducted by comparing the performance of BNC-5 (best performing sorbent) to milled-AC (most commonly used sorbent). The data in Fig. 7a and 7b shows the gradual decline in adsorption capacities after cycling the electrodes hundreds of times. With the chemical functionalization of BNC-5, there is a marked difference in the adsorption capacity compared to milled-AC, but also the number of electrode cycles at which 80% capacity retention is attained is extended for BNC-5 (440 cycles in $Cu^{2+}$; 420 cycles in

$Pb^{2+}$) compared to milled-AC (340 cycles in $Cu^{2+}$; 340 cycles in $Pb^{2+}$). Therefore, if the BNC-5 electrode continued to deteriorate at a similar rate (as identified by the dashed line), then approximately 700 electrode cycles could be achieved before the electroadsorption capacity matched the initial performance of milled-AC. This is a remarkable extension of sorbent lifetime, and demonstrates the tremendous performance advantage of the fabricated sorbent. Furthermore, both sorbents were regenerated using weak chemical treatment (Materials and Methods section) once 80% capacity retention was reached. Twice repeating the wash process led to over 1200 cycles being achieved for BNC-5 before the adsorption capacity dropped below 0.74 mmol $g^{-1}$, although the limit of this regeneration protocol (number of washes) to extending the number of cycles was not found. This long test (approximately 5 weeks to complete) highlighted the robustness of the fabricated material to voltage cycling and weak chemical treatment to extend the operational lifetime of the sorbent for use with CDI.

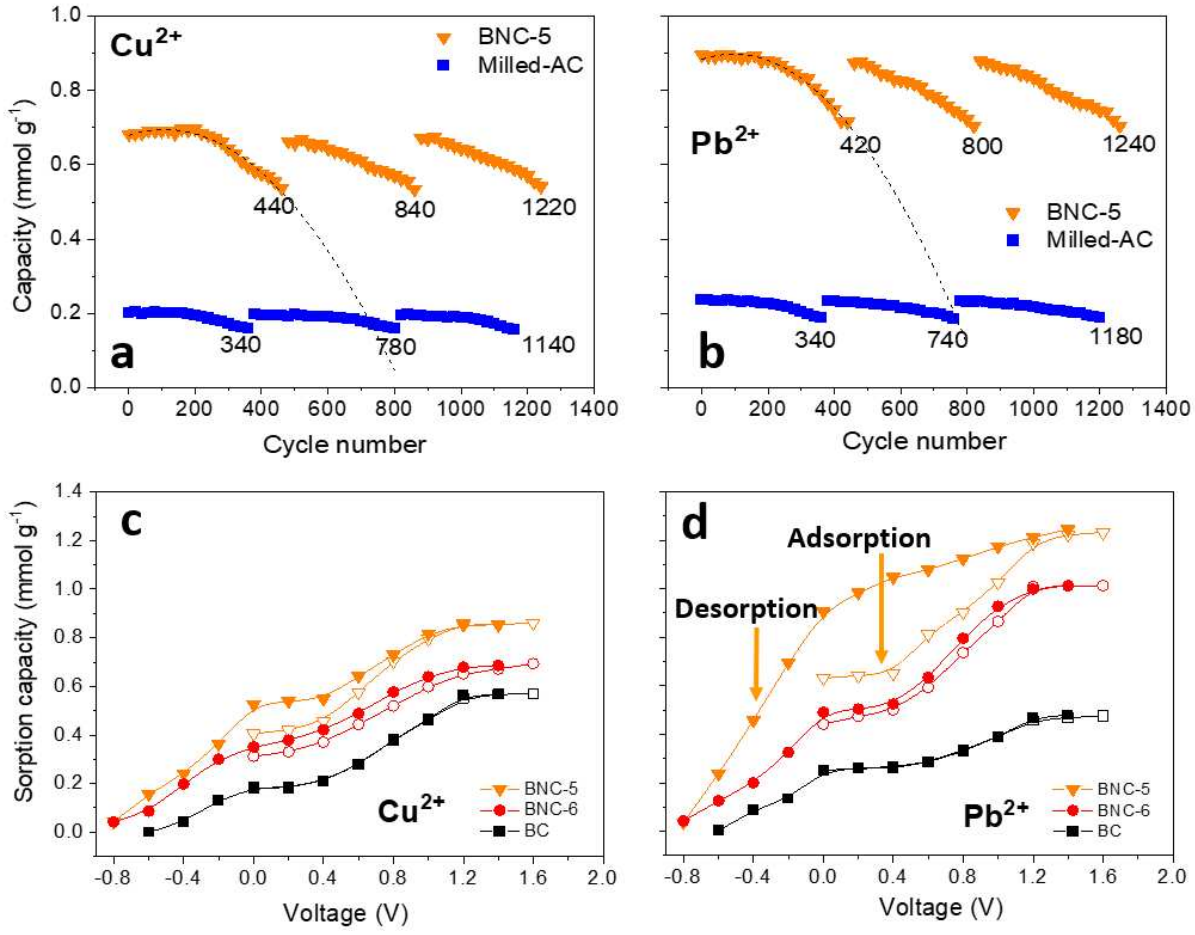

**Figure 7.** Long-term cycling performance of (a) BNC-5 and (b) milled-AC in 0.79 mmol $L^{-1}$ $Cu^{2+}$ or 0.24 mmol $L^{-1}$ $Pb^{2+}$. The cycling time was 10 min electroadsorption and 10 min electro-desorption. The electrodes were chemically regenerated using 0.1 M $HNO_3$ once 80% capacity retention was reached. The dashed line is added to guide the eye. The step-wise electrosorption capacity of $Cu^{2+}$ (c) and $Pb^{2+}$(d) by the fabricated electrode materials in CDI. The open symbols represent the electoadsorption data of increasing applied voltage while the solid symbols represent the electro-desorption data of decreasing applied voltage after electroadsorption at 1.6 V for 30 min. The initial concentration of the test fluid was 0.79 mmol $L^{-1}$ $Cu^{2+}$ or 0.24 mmol $L^{-1}$ $Pb^{2+}$.

The effect of applied voltages on electrosorption capacities of BC, BNC-5 and BNC-6 are shown in Fig. 7c and 7d. All samples showed a similar S-shaped characteristic when increasing the applied voltage. Between 0 and 0.4 V, the electroadsorption capacities showed negligible dependence on the applied voltage, thus the performance is mostly determined by physisorption and chemisorption, with the zeta potential of BC, BNC-5 and BNC-6 being −34 mV, −46.4 mV and −42.1 mV, respectively. Between 0.4 and 1.2 V, the electroadsorption capacities increased linearly with the applied voltage, demonstrating the strong influence of the electroadsorption effect. However, above 1.2 V the electroadsorption capacities plateaued, signifying saturation of the sorbent materials and that the full electroadsorption capacities had been reached.

To determine the nature of ion binding by each fabricated sorbent, electro-desorption experiments were conducted by reducing the applied voltage after electroadsorption at 1.6 V for 30 min. In the series of tests, the applied voltage was reduced to the desired level while the test solution was continuously cycled through the CDI cell for a further 30 min, before measuring the concentration of $Cu^{2+}$ or $Pb^{2+}$ in solution. For the BC sorbent, no hysteresis in

sorption capacity was observed between the adsorption-step and desorption-step. This contrasts the increasing hysteresis for BNC-6 and then BNC-5, with BNC-5 in $Pb^{2+}$ showing the largest hysteresis between the adsorption-step and desorption-step. For BC, such behavior likely confirms a physical adsorption process, with the energy of adsorption and desorption being equal. For the aniline functionalization (BNC-6), the sorption hysteresis was small but measurable in both $Cu^{2+}$ and $Pb^{2+}$ solutions, and likely indicates the ion binding to be both physical adsorption and weak chemical binding from the Lewis acid-base binding of $Cu^{2+}$ and $Pb^{2+}$ on BNC-6. With the same chemical binding expected with BNC-5, the large hysteresis for BNC-5 and $Pb^{2+}$ can be attributed to the strong binding energy between the soft base sites and soft acid ions. The effectiveness of the chemical selectivity is easily seen from the size of the hysteresis loop with the loop size decreasing in the order BNC-5-$Pb^{2+}$ > BNC-5-$Cu^{2+}$ > BNC-6-$Pb^{2+}$ > BNC-6-$Cu^{2+}$, and corresponds to the anticipated soft base interaction with soft acid metal ions. The results in Fig. 7c and 7d show almost full electro-desorption of the adsorbed metal ions from BNC-5 and BNC-6 at a sufficiently low voltage of −0.8 V for 30 min, thus achieving significant electrode regeneration without the need to use harsh chemicals. When combined with CDI, the fabricated sorbent provides an ideal route to safely treat contaminated water, minimize the amount of generated solids waste, and avoids the need to frequently use harsh chemicals, such as strong acids, that are typically needed to regenerate sorbents, but then require further treatment prior to disposal.

## Conclusions

Capacitive deionization is an emerging technology that overcomes many of the limitations of existing decontamination methods, and in future, has potential to be hybridized within a larger energy network to facilitate a cooperative system of wastewater treatment and energy generation[62]. With few large scale demonstrations of CDI, much effort is given to designing

better performing electrodes at low cost, thus creating a route to scale-up and commercialize the technology. The current study demonstrated a simple route to convert a food waste, pomelo peel, into a high-performance electrode for the selective removal of $Pb^{2+}$ and $Cu^{2+}$ from contaminated water. Although a full-economic assessment of the fabrication method is nontrivial, the biochar production cost per ton is comparable or better than typical sorbents such as activated carbon[63]. Furthermore, the superior performance of the fabricated electrode (BNC-5) compared to milled-AC, makes this route attractive to develop high-performance CDI electrodes.

Bio-based electrodes were fabricated by a simple two-step calcination process and functionalized with pyrrolic-N (BNC-5) and pyridinic-N (BNC-6) to remove $Pb^{2+}$ and $Cu^{2+}$ from contaminated water. Exploiting the mesoporous carbon structure and the Lewis acid-base interaction between soft acid ions and soft base adsorption sites, BNC-5 performed strongly to remove $Pb^{2+}$ and also proved successful in removing $Cu^{2+}$ from contaminated water compared to BNC-6 and the non-functionalized sorbent BC. Chemical functionalization led to a significant synergistic effect whereby the electroadsorption capacity for $Pb^{2+}$ at 1.2 V increased from $\sim$0.8 mmol $g^{-1}$ for BC to $\sim$2.0 mmol $g^{-1}$ for BNC-5. This substantial increase in electroadsorption capacity was attributed to the activation of the N-sites by the electric field, promoting high selectivity of $Pb^{2+}$ and the strong retention of the metal ions at these sites, as seen by a large hysteresis between the electroadsorption and electro-desorption profiles. Furthermore, near complete regeneration of the electrode was possible with an applied voltage of $-0.8$ V, and the electrode performance was shown to maintain its high performance over thousand adsorption-desorption cycles. The cycling robustness of the bio-based sorbent and its comparable performance to graphene-based sorbents demonstrate the potential of developing high performance materials from waste products in CDI. As environmental pressures build, there is a great emphasis on utilizing and converting wastes into valuable products, which has

been demonstrated in the current study.

## Supporting Information

Supporting Information is accessible via the link

## Acknowledgments

The authors would like to thank financial support from several organizations including: Shenzhen Key Laboratory of Interfacial Science and Engineering of Materials (Grant No. ZDSYS20200421111401738); Leading Talents of Guangdong Province Program (Z.X.; 2016LJ06C536); Core Research Facilities, SUSTech; The Engineering and Physical Sciences Research Council (EPSRC) (D.H. and T.N.H.; EP/S032797/1) the National Natural Science Foundation of China (F.Y.; 21808101) and Research Foundation for Advanced Talents (F.Y.; 20200207).

## References

[1] X. Yang, Y. Wan, Y. Zheng, F. He, Z. Yu, J. Huang, H. Wang, Y.S. Ok, Y. Jiang, B. Gao, Surface functional groups of carbon-based adsorbents and their roles in the removal of heavy metals from aqueous solutions: A critical review, Chem. Eng. J. 366 (2019) 608-621. https://doi.org/10.1016/j.cej.2019.02.119.
[2] Y. Vasseghian, F. Almomani, E.N. Dragoi, Health risk assessment induced by trace toxic metals in tap drinking water: Condorcet principle development, Chemosphere 286 (2021) 131821-131827. https://doi.org/10.1016/j.chemosphere.2021.131821.
[3] Q. Chen, Z. Luo, C. Hills, G. Xue, M. Tyrer, Precipitation of heavy metals from wastewater using simulated flue gas: Sequent additions of fly ash, lime and carbon dioxide, Water Res. 43 (2009) 2605-2614. https://doi.org/10.1016/j.watres.2009.03.007.
[4] M.Y. Vilensky, B. Berkowitz, A. Warshawsky, In situ remediation of groundwater contaminated by heavy- and transition-metal ions by selective ion-exchange methods, Environ. Sci. Technol. 36 (2002) 1851-1855. https://doi.org/10.1021/es010313.
[5] P.L. Yap, Y.L. Auyoong, K. Hassan, F. Farivar, D.N.H. Tran, J. Ma, D. Losic, Multithiol functionalized graphene bio-sponge via photoinitiated thiol-ene click chemistry for efficient heavy metal ions adsorption, Chem. Eng. J. 395 (2020) 124965. https://doi.org/10.1016/j.cej.2020.124965.
[6] J.E. Efome, D. Rana, T. Matsuura, C.Q. Lan, Experiment and modeling for flux and permeate concentration of heavy metal ion in adsorptive membrane filtration using a metal-

organic framework incorporated nanofibrous membrane, Chem. Eng. J. 352 (2018) 737-744. https://doi.org/10.1016/j.cej.2018.07.077.
[7] X. Liu, J. Wu, L.-a. Hou, J. Wang, Removal of Co, Sr and Cs ions from simulated radioactive wastewater by forward osmosis, Chemosphere 232 (2019) 87-95. https://doi.org/10.1016/j.chemosphere.2019.05.210.
[8] L. Liu, X. Guo, R. Tallon, X. Huang, J. Chen, Highly porous N-doped graphene nanosheets for rapid removal of heavy metals from water by capacitive deionization, Chem. Commun. 53 (2017) 881-884. https://doi.org/10.1039/c6cc08515f.
[9] C. Santhosh, V. Velmurugan, G. Jacob, S.K. Jeong, A.N. Grace, A. Bhatnagar, Role of nanomaterials in water treatment applications: A review, Chem. Eng. J. 306 (2016) 1116-1137. https://doi.org/dx.doi.org/10.1016/j.cej.2016.08.053.
[10] S. Porada, L. Borchardt, M. Oschatz, M. Bryjak, J.S. Atchison, K.J. Keesman, S. Kaskel, P.M. Biesheuvel, V. Presser, Direct prediction of the desalination performance of porous carbon electrodes for capacitive deionization, Energy Environ. Sci. 6 (2013) 3700-3712. https://doi.org/10.1039/c3ee42209g.
[11] M.E. Suss, S. Porada, X. Sun, P.M. Biesheuvel, J. Yoon, V. Presser, Water desalination via capacitive deionization: what is it and what can we expect from it?, Energy Environ. Sci. 8 (2015) 2296-2319. https://doi.org/10.1039/c5ee00519a.
[12] J. Li, X. Wang, H. Wang, S. Wang, T. Hayat, A. Alsaedi, X. Wang, Functionalization of biomass carbonaceous aerogels and their application as electrode materials for electro-enhanced recovery of metal ions, Environ. Sci. Nano 4 (2017) 1114-1123. https://doi.org/10.1039/c7en00019g.
[13] C.S. Fan, S.C. Tseng, K.C. Li, C.H. Hou, Electro-removal of arsenic(III) and arsenic(V) from aqueous solutions by capacitive deionization, J. Hazard. Mater. 312 (2016) 208-215. https://doi.org/10.1016/j.jhazmat.2016.03.055.
[14] M. Dai, L. Xia, S. Song, C. Peng, J.R. Rangel-Mendez, R. Cruz-Gaona, Electrosorption of As(III) in aqueous solutions with activated carbon as the electrode, Appl. Surf. Sci. 434 (2018) 816-821. https://doi.org/10.1016/j.apsusc.2017.10.238.
[15] Y.X. Liu, D.X. Yuan, J.M. Yan, Q.L. Li, T. Ouyang, Electrochemical removal of chromium from aqueous solutions using electrodes of stainless steel nets coated with single wall carbon nanotubes, J. Hazard. Mater. 186 (2011) 473-80. https://doi.org/10.1016/j.jhazmat.2010.11.025.
[16] L. Yang, Z. Shi, W. Yang, Enhanced capacitive deionization of lead ions using air-plasma treated carbon nanotube electrode, Surf. Coat. Technol. 251 (2014) 122-127. https://doi.org/10.1016/j.surfcoat.2014.04.012.
[17] Q. Ji, C. Hu, H. Liu, J. Qu, Development of nitrogen-doped carbon for selective metal ion capture, Chem. Eng. J. 350 (2018) 608-615. https://doi.org/10.1016/j.cej.2018.06.018.
[18] Y. Wei, L. Xu, K. Yang, Y. Wang, Z. Wang, Y. Kong, H. Xue, Electrosorption of toxic heavy metal ions by mono S-or N-doped and S, N-codoped 3D graphene aerogels, J. Electrochem. Soc. 164 (2017) E17-E22. https://doi.org/10.1149/2.1301702jes.
[19] S. Hou, X. Xu, M. Wang, T. Lu, C.Q. Sun, L. Pan, Synergistic conversion and removal of total Cr from aqueous solution by photocatalysis and capacitive deionization, Chem. Eng. J. 337 (2018) 398-404. https://doi.org/10.1016/j.cej.2017.12.120.
[20] G. Li, F. Yang, L. Wu, L. Qian, X. Hu, Z. Wang, W. Chen, Agricultural waste buckwheat husk derived bifunctional nitrogen, sulfur and oxygen-co-doped porous carbon for symmetric supercapacitors and capacitive deionization, New J. Chem. 45 (2021) 10432-10447. https://doi.org/10.1039/d1nj00579k.
[21] A. Benítez, J. Amaro-Gahete, Y.-C. Chien, Á. Caballero, J. Morales, D. Brandell, Recent advances in lithium-sulfur batteries using biomass-derived carbons as sulfur host, Renew. Sust. Energy Rev. 154 (2022) 111783. https://doi.org/https://doi.org/10.1016/j.rser.2021.111783.

[22] A. Fdez-Sanromán, M. Pazos, E. Rosales, M.A. Sanromán, Unravelling the environmental application of biochar as low-cost biosorbent: A review, Appl. Sci. 10 (2020) 7810. https://doi.org/10.3390/app10217810.
[23] M.S. Gaikwad, C. Balomajumder, A.K. Tiwari, Acid treated RHWBAC electrode performance for Cr(VI) removal by capacitive deionization and CFD analysis study, Chemosphere 254 (2020) 126781. https://doi.org/10.1016/j.chemosphere.2020.126781.
[24] F. Rouhani, A. Morsali, Fast and selective heavy metal removal by a novel metal-organic framework designed with in-situ ligand building block fabrication bearing free nitrogen, Chemistry 24 (2018) 5529-5537. https://doi.org/10.1002/chem.201706016.
[25] G. Yang, L. Tang, G. Zeng, Y. Cai, J. Tang, Y. Pang, Y. Zhou, Y. Liu, J. Wang, S. Zhang, W. Xiong, Simultaneous removal of lead and phenol contamination from water by nitrogen-functionalized magnetic ordered mesoporous carbon, Chem. Eng. J. 259 (2015) 854-864. https://doi.org/10.1016/j.cej.2014.08.081.
[26] Y. Gao, Z. Li, Z. Fu, H. Zhang, G. Wang, H. Zhou, Highly selective capacitive deionization of copper ions in FeS2@ N, S co-doped carbon electrode from wastewater, Sep. Purif. Technol. 262 (2021) 118336. https://doi.org/10.1016/j.seppur.2021.118336.
[27] Z. Jafari, V.M. Avargani, M.R. Rahimi, S. Mosleh, Magnetic nanoparticles-embedded nitrogen-doped carbon nanotube/porous carbon hybrid derived from a metal-organic framework as a highly efficient adsorbent for selective removal of Pb(II) ions from aqueous solution, J. Mol. Liq. 318 (2020) 113987. https://doi.org/10.1016/j.molliq.2020.113987.
[28] H.T. Fan, X.T. Sun, Z.G. Zhang, W.X. Li, Selective removal of lead(II) from aqueous solution by an ion-imprinted silica sorbent functionalized with chelating N-donor atoms, J. Chem. Eng. Data 59 (2014) 2106-2114. https://doi.org/10.1021/je500328t.
[29] J. Tang, Y. Chen, M. Zhao, S. Wang, L. Zhang, Phenylthiosemicarbazide-functionalized UiO-66-$NH_2$ as highly efficient adsorbent for the selective removal of lead from aqueous solutions, J. Hazard. Mater. (2021) 125278. https://doi.org/10.1016/j.jhazmat.2021.125278.
[30] K. Nakamoto, M. Ohshiro, T. Kobayashi, Mordenite zeolite—Polyethersulfone composite fibers developed for decontamination of heavy metal ions, J. Environ. Chem. Eng. 5 (2017) 513-525. https://doi.org/10.1016/j.jece.2016.12.031.
[31] W. Zheng, S. Chen, H. Liu, Y. Ma, W. Xu, Study of the modification mechanism of heavy metal ions adsorbed by biomass-activated carbon doped with a solid nitrogen source, RSC Adv. 9 (2019) 37440-37449. https://doi.org/10.1039/c9ra07191a.
[32] J. Chen, M. Yuan, W. Cai, J. Wei, J. Zhou, P. Liu, Z. Yang, J. Luo, Q. Xia, Z. Cai, Constructing the frustrated Lewis pairs within N, S-codoped carbon to reveal the role of adjacent heteroatom sites for highly effective removal of heavy metal ions, Chem. Eng. J. 422 (2021) 130153. https://doi.org/10.1016/j.cej.2021.130153.
[33] McMurry, John, Organic chemistry / 7th ed, Organic chemistry / 7th ed.
[34] S.Y. Huang, C.S. Fan, C.H. Hou, Electro-enhanced removal of copper ions from aqueous solutions by capacitive deionization, J. Hazard. Mater. 278 (2014) 8-15. https://doi.org/10.1016/j.jhazmat.2014.05.074.
[35] F.L. Chengzhi Hu, Huachun Lan, Huijuan Liu, Jiuhui Qu, Preparation of a manganese dioxide carbon fiber electrode for electrosorptive removal of copper ions from water, J. Colloid Interface Sci. 446 (2015) 359–365. https://doi.org/10.1016/j.jcis.2014.12.051.
[36] S. Wu, P. Yan, W. Yang, J. Zhou, H. Wang, L. Che, P. Zhu, $ZnCl_2$ enabled synthesis of activated carbons from ion-exchange resin for efficient removal of $Cu^{2+}$ ions from water via capacitive deionization, Chemosphere 264 (2021) 128557. https://doi.org/10.1016/j.chemosphere.2020.128557.
[37] R. Wang, B. Xu, Y. Chen, X. Yin, Y. Liu, W. Yang, Electro-enhanced adsorption of lead ions from slightly-polluted water by capacitive deionization, Sep. Purif. Technol. (2021) 120122. https://doi.org/10.1016/j.seppur.2021.120122.
[38] P. Liu, T. Yan, J. Zhang, L. Shi, D. Zhang, Separation and recovery of heavy metal ions

and salt ions from wastewater by 3D graphene-based asymmetric electrodes via capacitive deionization, J. Mater. Chem. A 5 (2017) 14748-14757. https://doi.org/10.1039/c7ta03515b.
[39] Z. Huang, L. Lu, Z. Cai, Z.J. Ren, Individual and competitive removal of heavy metals using capacitive deionization, J. Hazard. Mater. 302 (2016) 323-331. https://doi.org/10.1016/j.jhazmat.2015.09.064.
[40] Y. Wei, L. Xu, Y. Tao, C. Yao, H. Xue, Y. Kong, Electrosorption of lead ions by nitrogen-doped graphene aerogels via one-pot hydrothermal route, Ind. Eng. Chem. Res. 55 (2016) 1912-1920. https://doi.org/10.1021/acs.iecr.5b04142.
[41] R. Tocmo, J. Pena-Fronteras, K.F. Calumba, M. Mendoza, J.J. Johnson, Valorization of pomelo (Citrus grandis Osbeck) peel: A review of current utilization, phytochemistry, bioactivities, and mechanisms of action, Compr. Rev. Food Sci. Food Saf. 19 (2020) 1969-2011. https://doi.org/10.1111/1541-4337.12561.
[42] Y. Ren, C. Chang, P. Wang, Pomelo peel modified with citrate as a sustainable adsorbent for removal of methylene blue from aqueous solution, Molecules 23 (2018) 1342-1352. https://doi.org/10.3390/molecules23061342.
[43] J. Li, H. Bai, X. Li, W. Li, J. Zhai, M. Li, G. Xi, Hierarchical porous carbon microspheres with superhydrophilic surface for efficient adsorption and detection of water-soluble contaminants, J. Mater. Chem. A 6 (2018) 12153-12161. https://doi.org/10.1039/C8TA02143K.
[44] Haizhen, Sun, Zebin, Zhang, Li, Tian, Yaxi, Cui, Guijia, Yan, A cost-effective porous carbon derived from pomelo peel for the removal of methyl orange from aqueous solution, Colloid. Surface. A 489 (2016) 191-199. https://doi.org/10.1016/j.colsurfa.2015.10.041.
[45] Y. Liu, S. Cao, C. Xi, H. Su, Z. Chen, A new nanocomposite assembled with metal organic framework and magnetic biochar derived from pomelo peels: A highly efficient adsorbent for ketamine in wastewater, J. Environ. Chem. Eng. 9 (2021) 106207. https://doi.org/10.1016/j.jece.2021.106207.
[46] P. Tasaso, Adsorption of copper using pomelo peel and depectinated pomelo peel, J. Clean Energy Technol. (2014) 154-157. https://doi.org/10.7763/jocet.2014.v2.112.
[47] Y. Chen, Y. Liu, Y. Li, Y. Chen, Y. Wu, H. Li, S. Wang, Z. Peng, R. Xu, Z. Zeng, Novel magnetic pomelo peel biochar for enhancing Pb(II) And Cu(II) adsorption: performance and mechanism, Water. Air. Soil Pollut. 231 (2020). https://doi.org/10.1007/s11270-020-04788-4.
[48] T. Zhao, Y. Yao, D. Li, F. Wu, C. Zhang, B. Gao, Facile low-temperature one-step synthesis of pomelo peel biochar under air atmosphere and its adsorption behaviors for Ag(I) and Pb(II), Sci. Total Environ. 640-641 (2018) 73-79. https://doi.org/10.1016/j.scitotenv.2018.05.251.
[49] D. Xu, Y. Tong, T. Yan, L. Shi, D. Zhang, N,P-Codoped meso-/microporous marbon merived from biomass materials via a dual-activation strategy as high-performance electrodes for deionization capacitors, Acs Sustain. Chem. Eng. 5 (2017) 5810-5819. https://doi.org/10.1021/acssuschemeng.7b00551.
[50] F. Gao, G. Shao, J. Qu, S. Lv, Y. Li, M. Wu, Tailoring of porous and nitrogen-rich carbons derived from hydrochar for high-performance supercapacitor electrodes, Electrochim. Acta 155 (2015) 201-208. https://doi.org/10.1016/j.electacta.2014.12.069.
[51] H. Chen, J. Lin, N. Zhang, L. Chen, S. Zhong, Y. Wang, W. Zhang, Q. Ling, Preparation of MgAl-EDTA-LDH based electrospun nanofiber membrane and its adsorption properties of copper(II) from wastewater, J. Hazard. Mater. 345 (2018) 1-9. https://doi.org/10.1016/j.jhazmat.2017.11.002.
[52] F. Fu, L. Xie, T. Bing, W. Qi, S. Jiang, Application of a novel strategy—Advanced Fenton-chemical precipitation to the treatment of strong stability chelated heavy metal containing wastewater, Chem. Eng. J. 189-190 (2012) 283-287. https://doi.org/10.1016/j.cej.2012.02.073.
[53] M. Biswal, A. Banerjee, M. Deo, S. Ogale, From dead leaves to high energy density

supercapacitors, Energy Environ. Sci. 6 (2013) 1249-1259. https://doi.org/10.1039/c3ee22325f.
[54] M.G. Lu, X.S. Zhao, Nanoporous materials: science and engineering, imperial college press (2004). https://doi.org/10.1142/9781860946561.
[55] P. Liu, T. Yan, L. Shi, H.S. Park, X. Chen, Z. Zhao, D. Zhang, Graphene-based materials for capacitive deionization, J. Mater. Chemi. A 5 (2017) 13907-13943. https://doi.org/10.1039/C7TA02653F.
[56] Y. Liu, R. Fu, Z. Lou, W. Fang, Z. Wang, X. Xu, Preparation of functional carbon-based materials for removal of heavy metals from aqueous solution, Prog. Chem. 27 (2015) 1665-1678. https://doi.org/10.7536/pc150401.
[57] Y. Zhou, X. Xu, B. Shan, Y. Wen, T. Jiang, J. Lu, S. Zhang, D.P. Wilkinson, J. Zhang, Y. Huang, Tuning and understanding the supercapacitance of heteroatom-doped graphene, Energy Stor. Mater. 1 (2015) 103-111. https://doi.org/10.1016/j.ensm.2015.09.002.
[58] H. Zhang, Y.K. Kim, T.N. Hunter, A.P. Brown, J.W. Lee, D. Harbottle, Organically modified clay with potassium copper hexacyanoferrate for enhanced $Cs^{+}$ adsorption capacity and selective recovery by flotation, J. Mater. Chem. A 5 (2017) 15130-15143. https://doi.org/10.1039/c7ta03873a.
[59] H. Sigel, R. Griesser, B. Prijs, D.B. Mccormick, M.G. Joiner, "Hard and soft" behavior of $Mn^{2+}$, $Cu^{2+}$, and $Zn^{2+}$ with respect-to carboxylic acids and α-oxy- or α-thio-substituted carboxylic acids of biochemical significance, Arch. Biochem. Biophys. 130 (1969) 514-520. https://doi.org/10.1016/0003-9861(69)90064-2.
[60] J. Wang, X. Sun, Olivine $LiFePO_4$: the remaining challenges for future energy storage, Energy Environ. Sci. 8 (2015) 1110-1138. https://doi.org/10.1039/c4ee04016c.
[61] J. de Rojas, A. Quintana, A. Lopeandia, J. Salguero, B. Muniz, F. Ibrahim, M. Chshiev, A. Nicolenco, M.O. Liedke, M. Butterling, A. Wagner, V. Sireus, L. Abad, C.J. Jensen, K. Liu, J. Nogues, J.L. Costa-Kramer, E. Menendez, J. Sort, Voltage-driven motion of nitrogen ions: a new paradigm for magneto-ionics, Nat. Commun. 11 (2020) 5871. https://doi.org/10.1038/s41467-020-19758-x.
[62] J. Landon, X. Gao, A. Omosebi, K. Liu, Progress and outlook for capacitive deionization technology, Curr. Opin. Chem. Eng. 25 (2019) 1-8. https://doi.org/10.1016/j.coche.2019.06.006.
[63] P. Krasucka, B. Pan, Y. Sik Ok, D. Mohan, B. Sarkar, P. Oleszczuk, Engineered biochar – A sustainable solution for the removal of antibiotics from water, Chem. Eng. J. 405 (2021) 126926. https://doi.org/10.1016/j.cej.2020.126926.